Clays and Clay Minerals, Vol. 45, No. 3, 390–403, 1997.

ILLITE–SMECTITE ALTERATION AND ACCOMPANYING REACTIONS IN A PENNSYLVANIAN UNDERCLAY STUDIED BY TEM

F. ELSASS,[1] J. ŚRODOŃ[2] AND M. ROBERT[1]

[1] Station de Science du Sol INRA, Route de Saint-Cyr, 78000 Versailles, France

[2] Institute of Geological Sciences PAN, Senacka 1, 31-002 Kraków, Poland

Abstract—Pennsylvanian underclay from Illinois is characterized by well-developed mineral zonation: towards the coal bed, marly limestone gradually evolves into carbonate-free clay, chlorite becomes undetectable and illite/smectite changes from ordered and illite-dominated into random and smectite-dominated, with both types present in the middle of the profile. Transmission electron microscopy (TEM) observations of the bulk material imply that disappearance of calcite is due to dissolution. Movement of SiO_2 in the upper part of the profile is evidenced by quartz cementation of clay aggregates; crystallization of kaolinite, by the presence of vermicular aggregates absent from less-altered samples. Illitic material in unaltered (limestone) samples consists of rare, large, Al-rich crystals of mica, interpreted as detrital, and abundant thin crystals of illite/smectite intimately mixed in approximately equal proportions with even thinner crystals of discrete illite. Both are more Mg- and Fe-rich than the large mica crystals and are interpreted as diagenetic, based on their $1M_d$ polytype and the correlation with coal rank. Illitic material of the upper, carbonate-free section of the profile contains the same 3 types of crystals, but in different proportions: illite/smectite crystals dominate and their composition is more smectitic. Two distinct morphologies of the aggregates of crystals with different proportions of the component layers are observed. It explains why 2 different illite/smectites are detectable by X-ray diffraction (XRD) in these samples. The analysis of chemical data suggests that the underclay is a residue after dissolution of all of the calcite and half of the quartz from the original limestone (paleosol and/or telogenetic process). The TEM observations are not decisive regarding the origin of variation within the illitic material. It may result from burial diagenetic illitization of more-smectitic material, similar to the composition preserved in the center of underclay profile, or it may represent telogenetic alteration of illitic clay by acid waters penetrating down from the coal bed. The aggradation model explains the increase in percent K_2O, MgO and illite layers in the uppermost part of the profile. Whichever is the direction of reaction, it proceeds on an aggregate-by-aggregate basis and not fundamental particle-by-particle, and cannot be explained by simple opening or collapse of interlayers.

Key Words—Coal Basin, Diagenesis, HRTEM, Illite/Smectite, Paleosol, Underclay, Weathering.

INTRODUCTION

Evolution of smectitic clays towards illite, which dominates diagenetic clay reactions, has been studied intensely by XRD since the 1960s. Recently, many new ideas have emerged in this field, inspired by the introduction of electron microscopy techniques (Nadeau et al. 1984; Ahn and Peacor 1986; Bell 1986; Klimentidis and Mackinnon 1986; Vali and Koster 1986; Eberl and Środoń 1988; Inoue et al. 1988; Środoń et al. 1990; Lanson and Champion 1991; Środoń et al. 1992).

The mechanism of reaction in the opposite direction, characteristic of weathering environments—that is, alteration of illitic clays to more-smectitic compositions—is less well understood. Soil scientists have concentrated their attention on chemical studies of K release, but mainly on coarse-grained minerals such as micas and feldspars (Romero et al. 1992; Hinsinger et al. 1993; reviews by Robert 1987; and Scott 1987). Potassium release from illite was studied also, but XRD documentation of this process is not very detailed (White 1951; Tomita and Dozono 1972; Robert 1973; Tributh et al. 1987). The same is true for electron microscope studies, as observed by Jiang et al. (1990). These authors interpreted their detailed TEM and atomic emission microscopy (AEM) observations of illite–rectorite assemblage as indicating illite degradation reaction, but most other authors consider these minerals as low-temperature metamorphic assemblages, characteristic of organic-rich shales (Paradis et al. 1983 and literature cited therein).

Most students of weathering argue in favor of transformation reactions involving the formation of intermediate mixed-layer clays, due to the release of K and gradual opening of illite interlayers into vermiculite or smectite interlayers, depending on the charge density of the silicate layers (Robert 1973). Rarely, other opinions can be found in soil literature, for example, crystallization of smectite or palygorskite at the expense of illite in alkaline environment (Tributh et al. 1987; Suarez et al. 1994) or K release by dissolution of illite (Feigenbaum and Shainberg 1975).

An unusual case of an illite–smectite reaction, recorded in profiles of a Pennsylvanian underclay from

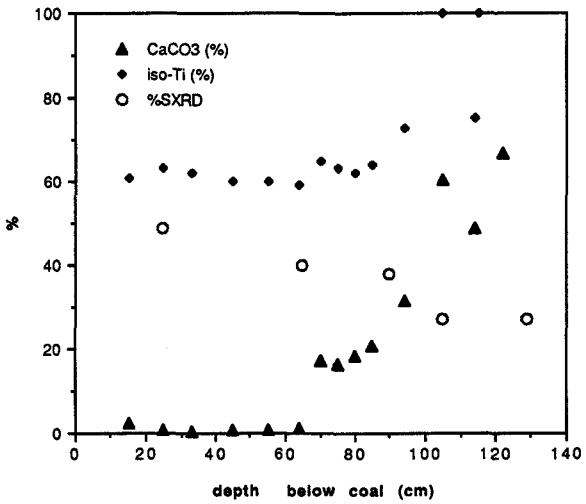

Figure 1. Major mineralogical variations in the underclay profile. Key: $CaCO_3$ = calcite content of the rock, calculated from CaO data of Rimmer (1978); Iso-Ti = mass of carbonate-free fraction, calculated from Rimmer (1978) bulk chemical analyses assuming conservation of Ti; and $\%S_{XRD}$ = XRD expandability of I/S in samples used in this study (from Table 1).

Illinois, was described by Rimmer (1978), Rimmer and Eberl (1982) and Środoń and Eberl (1984), who interpreted it as a result of acid alteration. In these rocks, 2 mixed-layer illite/smectites, identified by XRD as random (R0) and R1-ordered, were found together, along with discrete illite, in numerous samples. Similar occurrences are known from hydrothermal environments (Beaufort and Meunier 1983—misinterpreted as R0 plus K-beidellite assemblage; Bouchet et al. 1988; Inoue et al. 1992), but they are uncommon. In this contribution, we report a study of the underclay samples by electron microscope techniques, undertaken in order to see how the fundamental particles of illite and smectite have to be arranged to produce such specific XRD characteristics and to shed some light on the formation mechanism of such clays.

MATERIALS

Underclays (called "Stigmaria soils" in Europe) are paleosols, common as members of depositional cyclothems of coal-bearing formations. They are nonbedded or have bedding heavily disturbed by bioturbation, and are rich in organic material, particularly in Stigmaria roots. They are typically claystones or mudstones, most often underlying coal beds, and having gradational contacts with sediments below. In relation to clay mineralogy, underclays represent a broad spectrum from plastic clays, dominated by illite and swelling minerals, to kaolinite, boehmite and diaspore-rich rocks (Huddle and Patterson 1961).

The plastic underclay studied by Rimmer and Eberl (1982) underlies the Herrin (no. 6) coal bed of the Carbondale Formation (Pennsylvanian of the Illinois Basin, midwestern United States). This study uses core samples (Core 1) from 1.3 m thick profile, located not deeper than 140 ft below ground (D. M. Moore, personal communication), in Madison County, Illinois, approximately 30 mi northeast of St. Louis, Missouri. In this profile and in several other profiles of the same underclay bed, Rimmer and Eberl documented the following systematic mineral variation:

At the bottom of the profile, the rock is a marly limestone (>50% calcite, Figure 1) and also contains quartz, plagioclase, pyrite and clay minerals: illite, ordered illite/smectite, kaolinite and chlorite. Toward the coal bed, the rock becomes clay-rich: contents of calcite, pyrite and chlorite gradually decrease to undetectable levels, gypsum appears and illite/smectite evolves from illite-dominated and R1 to smectite-dominated and R0 via intermediate mixtures of R0 and R1 minerals. This specific evolution of illite/smectite clay, detected in <2 μm fraction, was confirmed by Środoń and Eberl (1984), who studied <0.2 μm fractions of the same samples.

Samples 1-6, 1-17, 1-23, 1-26 and 1-31, representing the complete range of variation in the profile (Table 1), were selected for electron microscope study.

Table 1. XRD identification of I/S in the <0.2 μm fraction of the studied underclay samples. Three %S values are given for sample 1-6, based on the peak position measured in the center and at the edges (parentheses) of the top plateau of the peak (see text).

Sample	Depth below coal (cm)	Analytical reflections	(°2θ)	%S	Type of ordering
1-31	131	6.84	—	27	R1
1-26	107	6.84	—	27	R1
1-23	90	6.56	—	38	R1 + R0 (trace)
1-17	65	16.43	31.93	40	R0 + R1
1-6	25	16.26	31.95	49	R0 + R1 (trace)
1-6	25	(15.93)	31.95	(80)	R0 + R1 (trace)
1-6	25	(16.53)	31.95	(35)	R0 + R1 (trace)

METHODS

Water-saturated chips of undisturbed bulk rocks and clay fractions were coated with agar, embedded in Spurr resin and sectioned by ultramicrotome. Under such experimental conditions, the illite layers remain collapsed at 1 nm and the smectite layers are intercalated by organic compounds, producing interlayer distances of about 1.35 nm. Images and elemental analyses of the ultrathin sections were obtained in a Philips 420 scanning transmission electron microscope (STEM) equipped with a LINK AN10000 energy dispersive system (EDS) using a windowless Si/Li detector. Details of the preparation and operating conditions for high-resolution microscopy are given in Środoń et al. (1990). Analytical conditions for elemental com-

https://doi.org/10.1346/CCMN.1997.0450309 Published online by Cambridge University Press

position are described in Romero et al. (1992). The analyses use *k*-factors normalized to Si concentration and calculated using K-saturated Llano vermiculite as a standard.

Micromorphology and elemental composition were obtained at 10,000× magnification in transmission mode on the bulk samples. Detailed studies of clay minerals were performed at 100,000× magnification in high-resolution mode on the bulk samples and the <0.2 μm fractions.

The thicknesses of sets of strictly parallel lattice fringes and the numbers of interlayers comprising sets were measured on negatives, using a binocular with a micrometric screw, which gives better precision than the 10× magnifying glass used in former studies (Środoń et al. 1990). More than 100 measurements were made for each sample. The magnification was calculated from multiple measurements of thick sericite crystals (Środoń et al. 1992, sample SG4).

XRD identification of clay minerals in samples studied by high-resolution TEM (HRTEM) was made using oriented preparations of <0.2 μm fractions. Identification of R1 illite/smectite clay in sample 1-26 was based on the position of its low-angle reflection (Środoń 1984, Figure 5). Identification of R0 illite/smectite was made using the 2-peak technique designed for mixtures of randomly interstratified illite/smectite and discrete illite (Środoń 1981). The 002/003 reflection of illite/smectite in sample 1-6 was very broad, with a plateau at the peak. Average and extreme illite:smectite compositions were determined, based on the center and the edges of the plateau (Table 1).

RESULTS

Textures and Mineral Compositions

Bulk samples 1-31, 1-26 and 1-23 contain abundant crystals of calcite, from 0.5 to a few μm in diameter, and always heavily corroded both at the edges and inside (Figure 2). They are absent from samples 1-17 and 1-6. Grains of apatite are of submicron size and are present in all samples except sample 1-6. All samples contain rare grains of quartz, up to 2 μm in diameter. In sample 1-6, a group of small natrojarosite crystals was detected by EDS (Table 2) and the presence of this mineral was confirmed by XRD.

Sheet silicates occur as subparallel aggregates of smaller particles up to a few μm long (Figure 2). The longest, the thickest and the most flat are aggregates of kaolinite crystals, present in all samples (Figure 2). Kaolinite crystals sometimes form parallel intergrowths with mica crystals of the same diameter and 10 or more layers thick. In sample 1-6, the thicknesses of kaolinite crystals are greater than their diameters and they contain packets of swelling interlayers (Figure 3). SiO_2 was found to form thick zones within such kaolinite crystals (Figure 3).

Muscovite mica crystals are rare but were found in all samples, in parallel associations with kaolinite or dispersed in the swelling clay matrix. They can be distinguished from illite or illite/smectite crystals by their shape and chemical composition. Mica crystals are more than 10 layers thick, flat, have strictly parallel sets of 1-nm layers, and are up to 1 μm long. They are almost free of Mg and Fe and sometimes rich in Na (Table 2).

Chlorite crystals are also rare but, unlike mica, they occur in separate aggregates (Figure 4). They are observed in all samples except sample 1-6. Crystals vary from a few to more than 10 layers in thickness. Chlorite is trioctahedral and Fe-rich (Table 2). Traces of CaO, Na_2O and K_2O indicate slight contamination of the analysis.

The remaining clay material of generally illitic composition is composed of very thin crystals (sets of strictly parallel layers only a few layers thick) grouped into large subparallel aggregates. The spacings between individual layers in these crystals are within the 1–1.4 nm range, but individual spacings cannot be measured precisely. In samples 1-31, 1-26 and 1-23, these aggregates have very similar morphologies (Figure 5). They are all relatively long and flat. In sample 1-17, a 2nd morphology is observed, which is dominant in sample 1-6: aggregates are much shorter and more curved, and on average individual crystals have more layers (Figure 6). Figure 7 illustrates the lateral transition between the 2 types of aggregates.

The aggregates have variable composition, differing from mica and chlorite by intermediate Fe and Mg content and also from mica by smaller K and Na contents and from chlorite analyses by much higher K (Table 2). In bulk sample 1-6, the illitic aggregates have Si contents that are too large for an illite/smectite composition. Irregularly shaped areas of pure SiO_2 are occasionally observed within clay aggregates. In the <0.2 μm fraction of this sample, the illitic aggregates do not contain excess SiO_2 (Table 2).

The clay particles from the <0.2 μm fraction are also subparallel aggregates of crystals as in the bulk rock, but they are on average thinner and shorter (compare Figure 8 with Figure 6). Two kinds of aggregate morphologies, in the bulk samples 1-17 and 1-6, can also be observed in the <0.2 μm fraction (Figure 8). Only $1M_d$ polytype of the illitic material was detected by XRD in bulk samples 1-6 and 1-26 (carbonate-free).

Chemical Composition of Illitic Aggregates

AEM analyses of fine-grained minerals must be interpreted with caution, because of possible admixture of other mineral phases. To eliminate the analyses of mixtures, a ternary diagram Si-Al-K/3 was used (K/3 instead of K, to obtain a better spread of the data

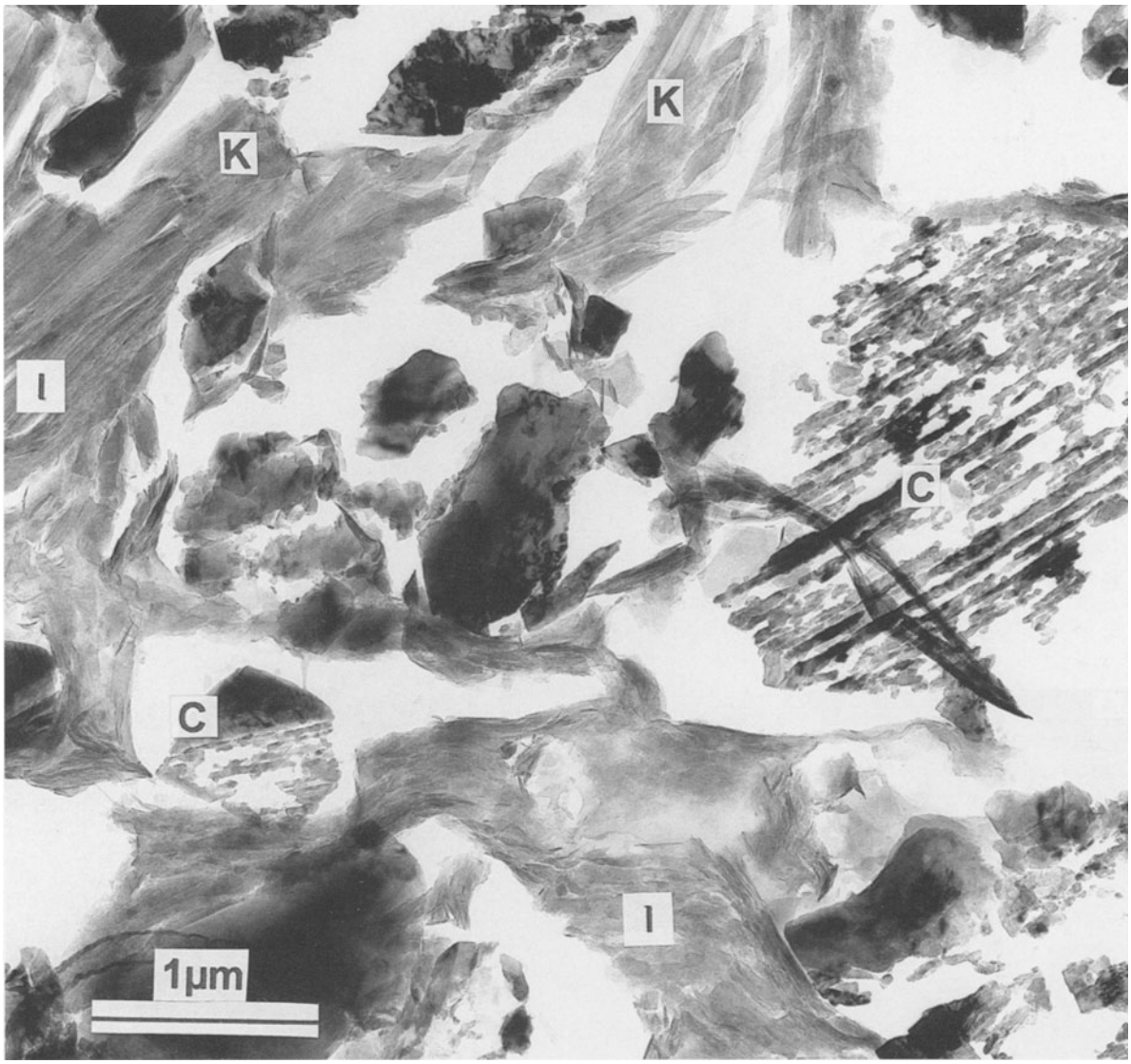

Figure 2. Sample 1-26 bulk. Corroded calcite crystals (C) and clay aggregates. The long and flat are kaolinite (K) and the less-regular are illite + illite/smectite (I).

points). Plots of pure minerals: quartz, K-feldspar, muscovite, illite (composition from Środoń et al. 1992), kaolinite, chlorite (composition from Table 2), low- and high-charge montmorillonite and beidellite are included in the diagram.

If all the analyses of illitic aggregates are plotted on the diagram (Figure 9), 3 groups of points are clearly separated. Noncontaminated analyses plot between the lines joining the illite pole with the smectite poles. The analyses of mixtures with SiO_2 plot to the left of this field, towards the quartz pole. These are only analyses of bulk sample 1-6; analyses of the <0.2 μm fraction of this sample plot within the I/S field. The analyses of mixtures with kaolinite and/or chlorite plot to the right, towards the projections of these minerals. The analyses of pure illitic aggregates from samples 1-6 and 1-26 are listed in Table 2.

The analyses of bulk sample 1-6 are corrected for SiO_2 admixture (20 to 60% of the mixture) based on the Al/K vs. Si/Al relationship established from the <0.2 μm fraction of this sample. The corrected analyses are plotted together with pure analyses in Figure 10. The following observations can be made:

1) Data points for samples 1-26, 1-23 and 1-17 are clustered between illite–montmorillonite and illite–beidellite lines within 25–60% smectite (S) compositional range.

2) Data for sample 1-6 are more spread, down to 75% S. The more smectitic compositions are shifted towards the montmorillonitic pole.

https://doi.org/10.1346/CCMN.1997.0450309 Published online by Cambridge University Press

Table 2. Selected AEM analyses of minerals in bulk samples (except for illitic material in sample 1-6: <0.2 μm), expressed as wt% oxides normalized to 100%.

Mineral	Chlorite	Mica	Mica	Natrojar.†	Illitic material		Ca-phosp.‡
Sample	1-23	1-6	1-17	1-6	1-26§	1-6#	1-31
SiO_2	32.37	64.48	51.00	9.92	58.23	57.14	0.08
Al_2O_3	24.13	24.49	35.20	6.24	30.23	29.84	0.18
Fe_2O_3	26.09	0.43	3.07	42.73	3.86	6.87	0.14
MgO	16.82	0.43	0.92	0.61	2.39	2.04	0.13
CaO	0.32	0.58	0.34	0.42	0.94	0.00	55.24
Na_2O	0.15	3.45	1.98	5.44	0.40	1.42	1.48
K_2O	0.13	6.15	7.48	1.43	4.10	3.18	0.60
SO_3	—	—	—	31.58	—	—	2.56
ClO_3	—	—	—	0.34	—	—	0.70
P_2O_5	—	—	—	1.29	—	—	38.87

† Natrojarosite.
‡ Ca-phosphate.
§ Average of 7 analyses.
# 1-μm spot.

Crystal Size Analysis of the Illitic Material

Detailed crystal size measurements are made for the bulk and <0.2 μm fractions of the samples 1-6 and 1-26, which represent the extreme expandabilities of the whole profile. The thickness (t) and the number of interlayers (n) are measured for each crystal. Data are presented in Table 3 as $T = \Sigma\, t$ (total thickness of all measured crystals), $N = \Sigma\, n$ (total number of interlayers in these crystals), and N_o = number of measured crystals (Środoń et al. 1990). From these data, 3 parameters defined in the cited paper are calculated: minimum expandability ($\%S_{MIN}$), that is, the percentage of smectitic interlayers within crystals, which should correspond to XRD expandability; maximum expandability ($\%S_{MAX}$), that is, the percentage of smectitic interlayers including crystal edges, which are assumed to be smectitic (each crystal edge counted as ½ of the smectitic interlayer); and the average number of interlayers per crystal (N/N_o).

The 1st calculations are made using all measurements, that is, regarding all data as representing 1 mixed-layer mineral. This assumption is inconsistent with XRD characteristics, which indicate the presence of illite/smectite mixed-layer clays and the discrete illite. In the 2nd approach, all measured crystals are classified into illite and illite/smectite populations. The thickness of 0.15 nm, that is, about half of the difference between illite (d = 1 nm) and smectite (d = 1.35

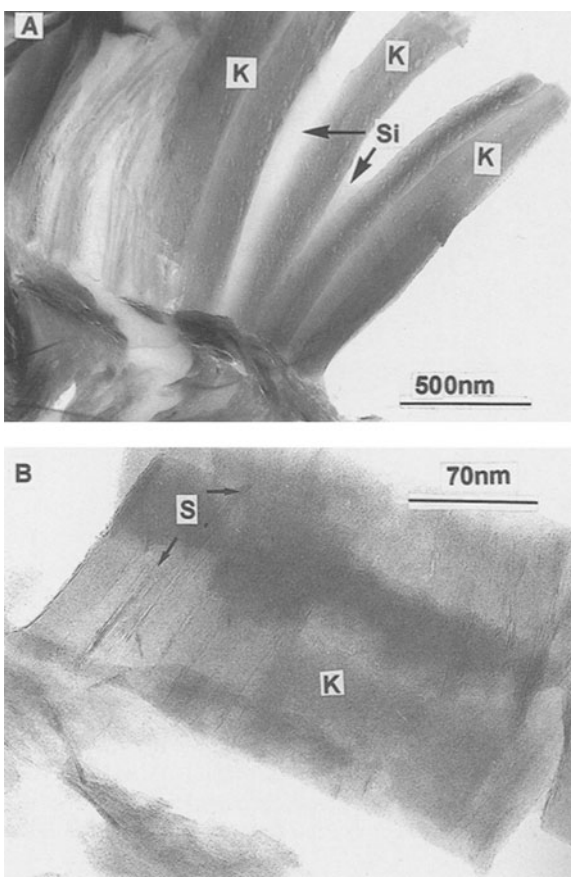

Figure 3. Sample 1-6 bulk. A) a book of kaolinite crystals (K) intergrown by 2 zones of SiO_2 (Si); B) thick kaolinite crystal (K) with groups of smectitic layers (S).

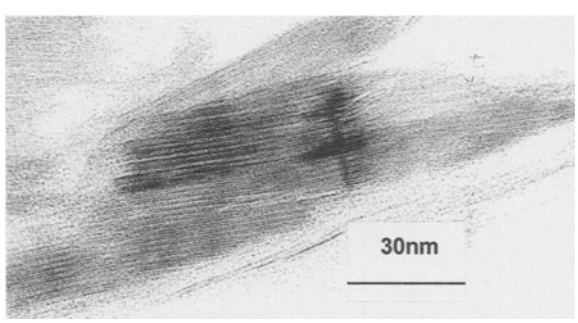

Figure 4. Sample 1-17 bulk. Aggregate of chlorite crystals.

https://doi.org/10.1346/CCMN.1997.0450309 Published online by Cambridge University Press

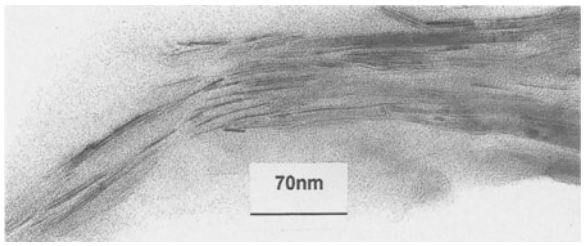

Figure 5. Sample 1-26 bulk. Long and flat subparallel aggregates of illite + I/S crystals. This morphology is present in all samples.

nm) spacing, was selected as the discriminating criterion (illite if $t < n + 0.15$, for t in nm).

The criterion was verified by applying it (Figure 11) to the crystal thickness data for a bentonitic sample having $\%S_{XRD}$ similar to sample 1-26, but devoid of free illite crystals detectable by XRD (sample R62 in Środoń et al. 1990). The proportion of illite crystals identified by this approach in sample R62 is well within the probabilities anticipated for such composition of R1 illite/smectite by the Marcovian statistics (74, 48, 31, 20, 13 and 9% of illite crystals for 1 to 6 interlayer crystallites, respectively; see Reynolds 1980, p 253). In sample 1-26, the use of the same criterion gives much higher proportions of illite crystals (Figure 11), in agreement with the XRD characteristics.

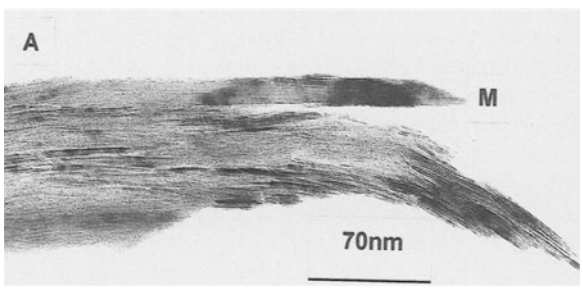

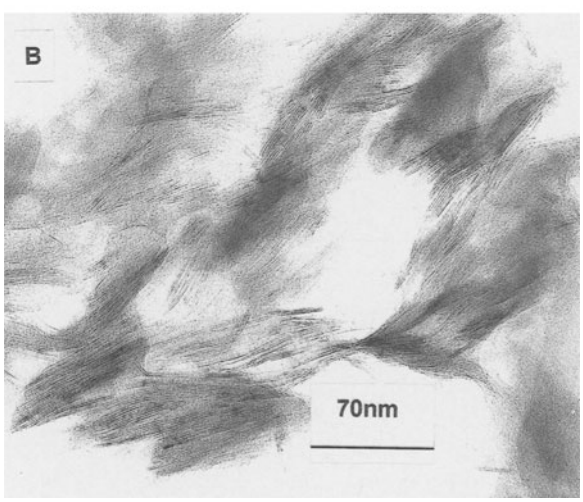

Figure 6. Sample 1-6 bulk. Two different morphologies of illite + I/S aggregates. Shorter and more curved aggregates (B) are more smectitic than longer, flat aggregates (A). Big mica crystal (M) in parallel association with A aggregates.

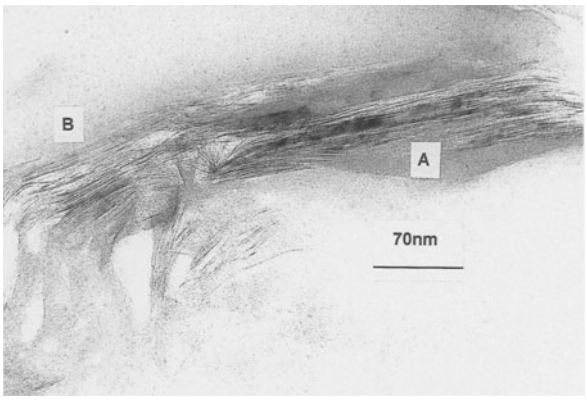

Figure 7. Sample 1-6 bulk. Transition between aggregate type A (more illitic) and B (more smectitic).

Table 3 contains the HRTEM data, the parameters calculated using these numbers and additionally the calculated weight percentages of illite and illite/smectite crystals. Figures 11 and 12 present crystal thickness distributions for the discrete illite and the mixed-layer fractions of the samples. From these data, the following observations can be made:

1) Calculation of $\%S_{MIN}$ for all crystals of the <0.2 μm fraction of sample 1-26 gives a much more illitic composition than $\%S_{XRD}$ of the mixed-layer fraction of this sample. This is as expected, because XRD detects much discrete illite in this sample. If the calculation is restricted to the population of mixed-layer crystals of this sample, the $\%S_{MIN}$ becomes more smectitic and well within the experimental error of XRD determination.

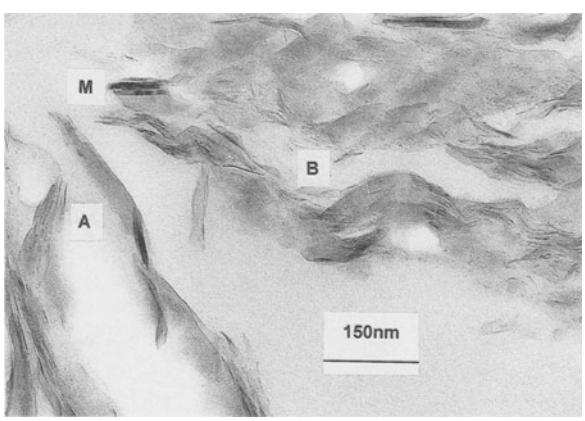

Figure 8. Sample 1-6 <0.2 μm fraction. The same difference in aggregate morphology as in Figure 6 is preserved in the fine clay fraction.

https://doi.org/10.1346/CCMN.1997.0450309 Published online by Cambridge University Press

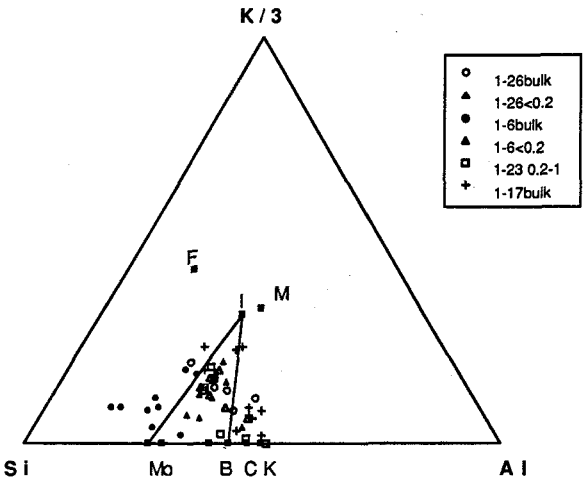

Figure 9. AEM analyses of illitic aggregates plotted on Si-Al-K/3 diagram in order to discriminate between analyses of pure illitic clay and mixture with other minerals. Theoretical compositions: F = Kspar, M = muscovite, I = illite, K = kaolinite, C = chlorite, Mo = montmorillonite, B = beidellite. Analyses of pure illitic aggregates are inside, analyses of mixtures with SiO_2 are to the left and analyses of mixtures with kaolinite or chlorite are to the right of illite–smectite triangle (I-Mo-B).

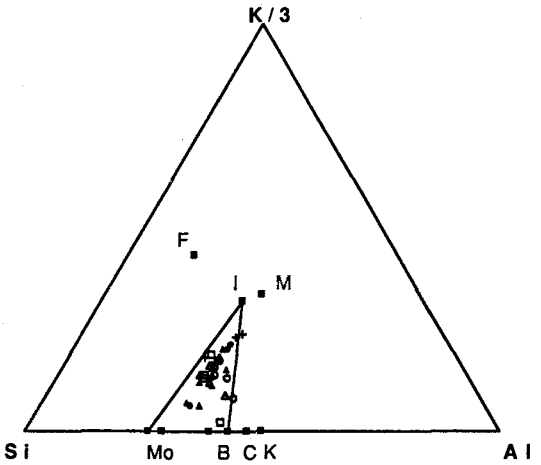

Figure 10. AEM analyses of pure illitic aggregates, including analyses corrected for admixture of SiO_2. See Figure 9 for explanation of symbols.

2) The mixed-layer components of the bulk and the <0.2 μm fraction of sample 1-26 have exactly the same $\%S_{MIN}$. This result indicates that in this sample the measurement of expandability made for the <0.2 μm fraction is representative of the whole rock. The agreement between XRD and HRTEM measurements of %S is consistent with earlier data obtained for bentonites (Środoń et al. 1990). It is taken as another proof that the applied criterion correctly discriminates between the populations of illite and illite/smectite crystals.

3) Sample 1-26 bulk is dominated by illite crystals, which are on average thinner than illite/smectite crystals (3.0 vs. 4.9 interlayers per crystal). The distributions of these 2 types of crystals are very different. The most frequent illite crystals are 1 interlayer (2 nm) thick and the distribution is highly skewed. The most frequent illite/smectite crystals are 3–4 interlayers thick and the distribution is less asymmetrical than the illite distribution.

4) In the <0.2 μm fraction of the same sample, illite and illite/smectite distributions preserve the same shapes; only the thickest (>11 interlayers) crystals disappear and illite/smectite crystals are markedly thinner (3.6 interlayers on average, 2–3 interlayers most frequent). Despite the fact that illite/smectite crystals are thicker than the illite ones, illite/smectite crystals accumulate in the <0.2 μm fraction, in agreement with the common experience of clay mineralogists (54 wt% illite/smectite in the illitic material of the <0.2 μm fraction against 43% in the bulk rock).

Table 3. Crystal thickness analysis of illitic material. ILL = illite crystals; I/S = illite/smectite; T = total thickness of all measured crystals; N = total number of interlayers; N_o = number of measured crystals; $\%S_{MIN}$ = % smectite calculated excluding crystal edges; $\%S_{MAX}$ = % smectite calculated including crystal edges.

	1-26 Bulk			1-26 <0.2 μm			1-6 Bulk			1-6 <0.2 μm		
	Total	ILL	I/S	Total	ILL	I/S	Total	ILL	I/S	Total	ILL	I/S
Measured values												
T (nm)	702.9	401.5	301.4	359.6	166.3	193.3	796.2	64.0	732.2	182.8	89.4	93.4
N	676	401	275	342	165	177	690	64	626	171	88	83
N_o	190	134	56	110	61	49	157	19	138	79	51	28
Monolayers	—	—	—	—	—	—	9	—	9	18	—	18
$\%S_{XRD}$	—	—	—	—	—	27	—	—	—	—	—	49
Calculated values												
$\%S_{MIN}$	10	—	27	15	—	26	44	—	48	20	—	36
$\%S_{MAX}$	31	25	40	36	29	42	55†	23	58†	49†	40	59†
N/N_o	3.6	3.0	4.9	3.1	2.7	3.6	4.4	3.4	4.5	2.2	1.7	3.0
Mass %	—	57	43	—	46	54	—	8	92	—	45	55

† Calculated accounting for monolayers, which were added to mixed-layer crystals.

https://doi.org/10.1346/CCMN.1997.0450309 Published online by Cambridge University Press

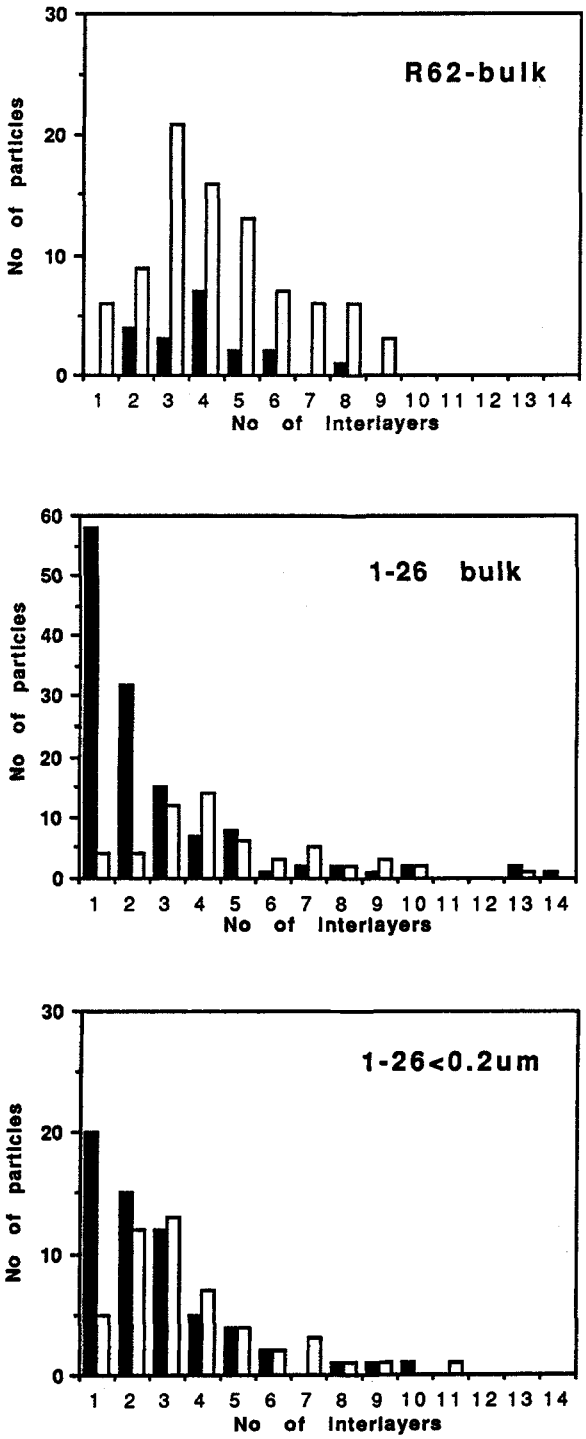

Figure 11. Histograms of crystal thickness (HRTEM measurements) for bentonite sample R62 ($\%S_{MAX}$ = 38%) free of discrete illite detectable by XRD and sample 1-26 bulk and <0.2 μm, both containing XRD-detectable discrete illite. Key: white bars = I/S crystals and black bars = illite crystals.

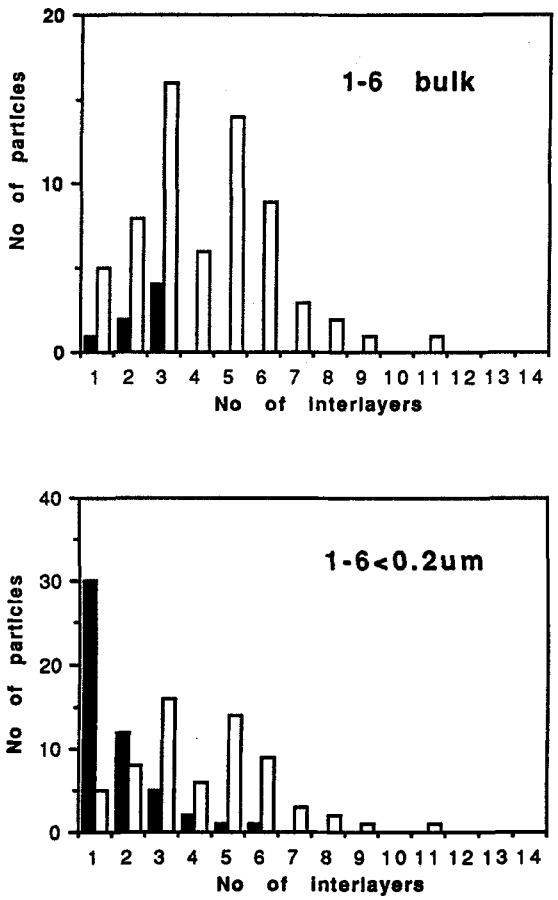

Figure 12. Histograms of crystal thickness (HRTEM measurements) for sample 1-6 bulk and <0.2 μm. Key: white bars = I/S crystals and black bars = illite crystals.

5) Bulk sample 1-6 is dominated by illite/smectite crystals: only 8% of the mass belongs to illite. A few monolayers were also spotted. Alternatively, the crystal thickness distributions are very similar to sample 1-26, including very close mean values. Again, illite crystals are definitely thinner than mixed-layer crystals. The $\%S_{MIN}$ for this sample is precisely equal to the value measured by XRD for the <0.2 μm fraction.

6) Illitic aggregates of different morphologies, observed in bulk sample 1-6, differ markedly in expandability of their mixed-layer fractions: long and flat aggregates have $\%S_{MIN}$ = 41 and short and curved aggregates are more smectitic: $\%S_{MIN}$ = 58. This variation is consistent with the XRD characteristics of this sample (Table 1): broadening and splitting of the 15.9–16.5 °2θ reflection and the presence of both the 1.7-nm reflection, indicating random mixed-layering, and the 2.7-nm reflection, indicating R1-ordered clay. This result can be contrasted with the behavior of the illite/smectite fraction of sample 1-26, which by XRD is a homogenous R1 mineral, and is built entirely of long and flat aggregates. The homogeneity of illite/smectite

https://doi.org/10.1346/CCMN.1997.0450309 Published online by Cambridge University Press

in this sample is checked by splitting the measurements into 2 populations and calculating $\%S_{MIN}$ for both of them. The difference is below 2% S.

7) The <0.2 μm fraction of sample 1-6 has characteristics very different from the bulk. The crystals are on average 2 times thinner, and 18% of them are monolayers (1 nm thick). Fifty-three percent of crystals are very thin illites, while in the bulk rock only 12% were illites, but they were exactly 2 times thicker. The $\%S_{MIN}$ of the mixed-layer fraction is, unlike sample 1-26, much smaller than in the bulk rock (36 vs. 48%). The $\%S_{MAX}$ calculated for all crystals and for mixed-layer fractions are, as in sample 1-26, very close to the values characterizing the bulk rock.

The $\%S_{MAX}$ characterizes the population of fundamental particles (in the sense of Nadeau et al. 1984) in the sample, whereas $\%S_{MIN}$ depends also upon their degree of association into crystals (Środoń et al. 1990). The values for sample 1-6 indicate that, in the bulk rock and <0.2 μm fraction, similar populations of fundamental particles are arranged into crystals in different manners. The big increase in number of very thin illitic particles in the <0.2 μm fraction, coupled with the marked decrease of the thickness of mixed-layer crystals, can be understood if we assume that, in the process of fraction separation from this sample, the mixed-layer crystals underwent partial infinite swelling along smectitic interlayers, thus liberating some fundamental particles and themselves becoming thinner (Figure 8). Fundamental particles in these crystals are much thinner than in the original illite crystal population (1.7 nm vs. 4.3 nm, Table 3). Their appearance as free illite crystals resulted in a shift of illite crystal population towards thinner crystals and in an increase of illite relative to mixed-layer crystals. Free monolayers are also produced in this process.

The above findings imply that illite/smectite crystals may not be entirely stable during the processes of standard clay fraction separation. Conclusions regarding the mechanism of clay alteration should not only be drawn from the TEM observations of clay crystals in the fractions, but also from the bulk rock studies.

The TEM characteristics of the <0.2 μm fraction of sample 1-6 do not agree with the XRD data: $\%S_{MIN}$ is smaller than $\%S_{XRD}$ (Table 3). This may imply that crystal splitting during separation is reversible and that, in the oriented XRD slide, crystals recombine to more or less original thickness ($\%S_{MIN}$ of the bulk sample very close to $\%S_{XRD}$ measured on the <0.2 μm fraction). A similar observation (XRD coherent scattering domain bigger than crystal thickness measured by HRTEM) was made by Sucha et al. (1996).

INTERPRETATIONS

Clay Mineralogy Unaffected by Underclay Alteration

Samples 1-26 and 1-31 represent the part of the profile almost unaffected by the alteration process that produced the underclay. It is documented by stable XRD (Table 1) and chemical (Rimmer 1978) characteristics of the bulk rocks from this part of the profile. The only alteration feature that can be attributed to the underclay alteration is the incipient dissolution of calcite crystals detected by TEM.

Electron microscope observations confirm XRD identification of 4 clay components of these marly limestone samples: kaolinite, trioctahedral chlorite, discrete illite and illite/smectite of about 26% smectitic interlayers ($\%S_{MIN}$).

The grain morphology provides no clues as to the origin of kaolinite: the crystals are relatively big, and may as well be detrital as authigenic. The chlorite mode of occurence indicates diagenetic origin. Small chlorite crystals are not dispersed in the mass of illitic material, as they would be if detrital, but are concentrated in chloritic aggregates (Figure 5). The Fe-rich composition is typical of diagenetic chlorites (Jahren and Aagaard 1992).

The dominant clay mass is composed of big subparallel aggregates of illitic material, containing both discrete illite and mixed-layer illite/smectite crystals and exhibiting XRD characteristics of mixed illite + illite/smectite assemblage, typical of the shale mineralogy. A surprising characteristic of this clay is that illite crystals are on average thinner than illite/smectite crystals. This observation is new in the literature and supports the interpretation of XRD data introduced by Lanson and Champion (1991). Other studies of coexisting illite/smectite and illite present evidence of relatively thick illite crystals, clearly distinct from the surrounding illite/smectite matrix (Ahn and Peacor 1986). More observations using our or similar embedding techniques, preserving the original fabric of the rock, are needed to evaluate this new case's frequency in nature. It must also be verified whether our 2 populations of crystals correspond to 2 populations of shape of fundamental particles (as in the case of laths vs. hexagons distinguished in samples of different lithologies from deep sections of the Paris Basin by Lanson and Champion 1991).

The origin of illite/smectite can be interpreted as diagenetic by comparison with known diagenetic profiles. Damberger (1971) classifies the coal overlying our profile (the Herrin bed) in the Madison County as high volatile C, with 16% H_2O and the calorific value of 12,100 BTu/lb. According to the correlative table of major organic indices of diagenetic grade (Bustin 1989), these parameters correspond to the vitrinite reflectance $R_o$max = 0.55% and the volatile matter content of 42%, which are typically found in young basins at approximately 1000 m of burial depth (Durand 1985; Taguchi et al. 1986). In the diagenetic profile of a Carboniferous basin in Poland, Środoń (1979) reported $\%S_{XRD}$ = 22–23 at $R_o$max = 0.7% and the volatile matter content of 38%. Comparison of the 2 sets

https://doi.org/10.1346/CCMN.1997.0450309 Published online by Cambridge University Press

Table 4. Chemical data used in the calculation of mineral composition. Chlorite and illite + illite/smectite (I + I/S) compositions are taken from Table 2.

Material	Non-carb. fraction of the bulk rock			Quartz	Kaolin.	Chlorite	Fe‡	I + I/S	
Sample	1-26	1-6	1-6†	—	—	—	—	1-26	1-6
SiO_2	76.05	71.16	45.32	100	54	33	0	58.23	57.14
Al_2O_3	13.06	18.30	11.66	0	46	24	0	30.23	29.84
Fe_2O_3	3.11	5.57	3.55	0	0	26	100	3.86	6.87
MgO	2.24	0.90	0.57	0	0	17	0	2.39	2.04
K_2O	1.20	1.53	0.97	0	0	0	0	4.10	3.18
TiO_2	0.68	1.07	0.68	—	—	—	—	—	—
Na_2O	3.65	1.48	0.94	—	—	—	—	—	—
Total	100.00	100.00	63.69	—	—	—	—	—	—

† Composition recalculated assuming conservation of TiO_2.
‡ Nonsilicate Fe minerals.

of data allows the conclusion that the marly limestone experienced in its diagenetic history temperatures that should have produced at least the level of illitization observed in the samples (presence of Ca significantly accelerates illitization of smectite; Small 1995).

Such reasoning by analogy as presented above is not possible for the discrete illite, which is commonly detectable all along the diagenetic profiles and is regarded as detrital (Hower et al. 1976) and/or diagenetic (Środoń 1979; Ahn and Peacor 1986; Amouric and Olives 1991). We suspect that, in this case, only the rare, large crystals of illite (mica) are detrital (Figure 6) and the fine illite crystals intimately mixed with illite/smectite crystals are diagenetic and cogenetic with the latter (both are $1M_d$ polytype). The fundamental particles of illite, which are components of the mixed-layer crystals, are on average thinner than the free illite crystals. Why diagenesis produced such heterogenous assemblages in this marly limestone, while leading to homogenous (that is, monomineral by XRD) assemblages in such rocks as K-bentonites (Figure 11) remains a question for further studies.

This result implies also that our present concept of interparticle diffraction (Nadeau et al. 1984) is an oversimplification. We would expect such thin illite crystals as present in sample 1-26 (mostly 2 or 3 nm thick) to produce the effect of mixed layering due to interparticle diffraction. Instead, a set of broad discrete illite reflections is observed (Środoń and Eberl 1984, Figure 19) beside the illite/smectite reflections. It has to be concluded that the small thickness of fundamental illite particles is not the only condition required to have them associating into mixed-layer crystals and producing XRD effect of illite/smectite interstratification (Środoń and Elsass 1994).

Mineral and Chemical Changes in the Underclay Profile

Rimmer (1978) presented 14 bulk rock major element analyses, confirming the total lack of calcite and apatite in the upper part of the profile. When these data are recalculated to 100% on a CaO-free basis (Table 5b), clear trends in chemical compositions can be observed up the profile starting from sample 1-26: 1) Al_2O_3 and TiO_2 increase; 2) Fe_2O_3 remains stable; and 3) SiO_2, MgO, Na_2O and K_2O decrease.

These vertical variations are well correlated with clear indications of dissolution reaction (calcite) and are typical of chemical trends in the weathering profiles (Garrels and Mackenzie 1971). It thus seems justified to try interpreting the whole profile not in terms of sedimentational differentiation, but as a result of postsedimentary alteration of a homogenous layer of marly limestone. In some locations, coals are known to directly overlie the limestone beds (Huddle and Patterson 1961).

The chemical trends in the underclay profile have to be interpreted in terms of an open system, as evidenced by the removal of huge amounts of calcite. Titanium appears as the most conservative element (enrichment of 1.6 at the top of the profile), which is typical of weathering alterations (Allen 1952). Assuming that Ti was fully conserved, the mass balance of the alteration reaction was calculated for all 14 analyses of Rimmer (1978). An example is presented in Table 4 for samples representative of original (1-26) and altered (1-6) rock. The following relations are observed: 1) Al and Fe are also conserved almost completely; 2) Si, Mg, K and Na are strongly depleted, but Mg and K increase again at the top of the profile; and 3) total mass loss of noncarbonate fraction of the rock is up to 40% (Figure 1).

Quantification of the mineralogical changes corresponding to these chemical trends can be attempted, based on the known chemical composition of the major mineral components: quartz, kaolinite, chlorite, illite + illite/smectite and Fe-containing minerals (pyrite, natrojarosite, iron oxyhydroxides). Illite and illite/smectite are grouped together in this calculation, because they occur in the same quasicrystals and the AEM averages their chemical composition. Table 4 presents all data used in these calculations.

Table 5. Mineral composition calculated from chemical data.

Sample	Quartz	Kaolinite	Chlorite	I + I/S	Fe‡	Σ
1-26	53	5	9	29	0	96
1-6 (K_2O)	39	9	0	48	2	98
1-6 (MgO)	40	11	0	44	3	98
1-6 (K_2O)†	25	6	0	31	1	63
1-6 (MgO)†	26	7	0	28	2	63

† Composition recalculated assuming conservation of TiO_2 (36% loss of mass).
‡ Nonsilicate Fe minerals.

First, the percentage of illite + illite/smectite (I + I/S) was calculated from $\%K_2O$. The result and %MgO were used to calculate percent chlorite (%Ch). In an alternative calculation for sample 1-6, %MgO was used to calculate I + I/S, assuming lack of chlorite in this sample. In the next step, I + I/S, Ch and $\%Al_2O_3$ gave the content of kaolinite (K). Finally, from $\%SiO_2$ and $\%Fe_2O_3$, the contents of quartz and Fe-containing minerals were obtained. The results are presented in Table 5.

The sums close to 100% confirm reliability of the calculation. The 2 techniques of calculation applied to sample 1-6 give only slightly different numbers, but the resulting apparent trends are the same. To interpret these changes in relative abundances within the noncarbonate fraction, the values of sample 1-6 have to be corrected for the weight loss relative to sample 1-26, which was calculated from the chemical data assuming stable TiO_2. The corrected values (Table 5) indicate that: 1) the alteration process did not significantly affect the mass of illite + illite/smectite; 2) the mass of kaolinite is slightly higher and the mass of quartz is 2 times lower in the altered zone; and 3) chlorite is present only in the unaltered zone, and nonsilicate iron minerals are present only in the altered zone.

The mass balance calculated assuming homogenous starting composition (marly limestone) and Ti conservation in the profile agrees well with the mineralogical observations: 1) the alteration of Fe-rich minerals took place in an oxidizing environment (natrojarosite), which explains the conservation of Fe; 2) lack of chlorite in the altered zone agrees with XRD and TEM observations; 3) some growth of kaolinite in the altered zone is documented by the observations of vermicular crystals, present only in sample 1-6; 4) large-scale dissolution of quartz or silicates is evidenced by SiO_2 impregnating clay quasicrystals and interlayering booklets of kaolinite only in sample 1-6.

Altogether, the postsedimentary alteration of the marly limestone removed 80% of the original mass of the rock.

Timing and Mechanism of the Alterations

Mineral reactions that have produced the present underclay profile may not have occurred all at the same time. The layer of marly limestone had a chance to be elevated into the zone of weathering just after deposition (the stage of paleosol development); later, it was buried and underwent diagenesis, and finally it was uplifted into the zone of telogenetic alterations by descending meteoric waters. When did the major processes take place?

Two reactions responsible for the bulk loss of mass of the original material are the dissolution of calcite and quartz. Both reactions are documented by TEM: the dissolution features in calcite crystals and silica cementation of clay aggregates. The curves in Figure 1 representing the dissolution of calcite and the weight loss of the carbonate-free fraction of the rock (which is almost equivalent to quartz dissolution, according to Table 5) are perfectly parallel. When calcite is completely dissolved, the weight of carbonate-free fraction is stabilized. These space relations suggest that quartz and calcite were dissolving in the same zone at the same time. This is not a common phenomenon and some special conditions have to be imagined. Dissolution of quartz in underclays has been observed earlier and interpreted as genuine soil process due to the action of Si-accumulating plants (calamites; Huddle and Patterson 1961). If we accept this interpretation, we have to assume that the dissolution features in calcite crystals survived diagenesis or that some additional dissolution of calcite has been taking place more recently.

An alternative interpretation is a telogenetic process. We can imagine oxidation of pyrite in the coal bed by meteoric waters and descending acid fluids altering the zone immediately under the coal: dissolving calcite, apatite and quartz (perhaps complexing by organic compounds as described by Bennett and Siegel 1987), and precipitating natrojarosite.

The reaction involving the illitic fraction of the rock is represented in Figure 1 by percent smectite layers in illite/smectite. It must be asked whether the underclay profile recorded the reaction proceeding from smectite to illite (aggradation) or in the opposite direction (degradation), or perhaps both phenomena superimposed. The HRTEM observations did not answer this question definitively, and all options have to be considered.

The aggradation model implies that sample 1-6 represents the composition of illitic fraction closest to the soil stage of the underclay development and that sample 1-26 represents the composition most altered by burial diagenesis. From the chemical standpoint, burial diagenesis of the thick bed deficient in K- and Mg-bearing minerals but rich in smectite could proceed in a manner similar to the diagenetic alteration of thick bentonite beds: K (and Mg) have to be imported from the outside (Parachoniak and Środoń 1974; Środoń 1976, 1979; Altaner et al. 1984), producing characteristic zonation: more smectitic clays in

the center of the bed. This model would explain the slight decrease of expandability (Środoń and Eberl 1984, Figure 18) and the increase in K_2O and MgO (Rimmer 1978, Table 5b) observed in the uppermost part of the underclay just below the coal, as well as the distribution of the 2nd diagenetic clay, chlorite (a byproduct of alteration of smectite into less Mg- and Fe-rich illite). The enrichment of K_2O and illite layers below the coal has been observed by Rimmer (1978) in her other profiles and reported by other authors (Huddle and Paterson 1961). The presence of natrojarosite can be explained by the aggradation model as a leftover of paleosol alteration in oxidizing conditions.

If the underclay profile recorded the smectite illitization reaction, the reaction mechanism was different from the one described for the zoned bentonite bed (Środoń et al. 1990). In the bentonite, illitization takes place inside mixed-layer crystals, on a fundamental particle-by-particle basis, producing homogenous mixed-layer illite/smectite without XRD-detectable discrete illite. In the underclay, we are observing 2 morphologies of aggregates, corresponding to 2 compositions of illite/smectite detectable by XRD. More than half of the clay mass is finally altered into discrete illite, the crystals of which are thinner than the mixed-layer crystals. It is difficult to imagine such reorganization without massive dissolution and recrystallization. Calculations (Table 5) indicate that the alteration process took place without much mass exchange with other phases. In particular, crystal size analysis shows that the coarse mica crystals (more than 10 layers thick) are very rare. According to AEM data, they most often underwent kaolinization, which is a common phenomenon in coal-bearing formations, well known to optical petrographers (Środoń 1972; Parachoniak and Środoń 1974).

An alternative interpretation of illite/smectite variation in the underclay profile is the "degradation model": reaction from illite to smectite. This is how the underclay profiles were interpreted by many previous workers including Huddle and Paterson (1961), Rimmer and Eberl (1982) and Hughes et al. (1992). In the investigated case, the reaction cannot be regarded as a soil process, because the potential starting material—that is, the illitic fraction of the limestone—is identified as a product of burial diagenesis. The alteration towards smectite could then have taken place only after burial, when the uplifted rocks found themselves again in contact with the surface. We would have to imagine the illite-to-smectite reaction accompanying the dissolution of quartz and calcite. The process of alteration of illitic material would proceed on an aggregate-by-aggregate and not crystal-by-crystal or fundamental particle-by-particle basis: while some aggregates are strongly affected, others are barely touched.

Crystal size analysis shows that this process could not have been simple opening of illite interlayers. Illite crystals, which dominate sample 1-26, are much thinner than mixed-layer crystals, which have similar thickness in both samples. Alteration of illite crystals of sample 1-26 into mixed-layer crystals could not produce the crystal thickness distribution measured for sample 1-6. Two processes could explain such crystal thickness distribution: 1) dissolution of small illite crystals and crystallization of bigger illite/smectite crystals; and 2) recombination of opened illite into bigger crystals: for example, if pairs of the most frequent 1 and 2 interlayer illite crystals were partially opened and—becoming more flexible—joined together face-to-face, we would obtain 3, 4 and 5 interlayer mixed-layer crystals, which are the most common in 1-6 clay.

The major difficulty of the degradation model is accounting for the increase of K_2O, MgO and %illite layers in illite/smectite at the top of the underclay.

CONCLUSIONS

1) The present-day mineral variation in the studied underclay profile records 2 or 3 superimposed phases of postsedimentary alteration: a) burial diagenesis, which produces very fine-grained illite, illite/smectite and chlorite; and b) paleosol development and/or telogenetic leaching, which removes all of the calcite and apatite and half of the quartz and produces some kaolinite. The telogenetic leaching could also affect the diagenetic clay minerals (growth of smectite and kaolinite at the expense of illite and chlorite).

2) Diagenesis (smectite to illite) or telogenesis (illite to smectite) superimposed on diagenesis are the processes responsible for the observed variation of illite/smectite composition in the profile. Whichever the direction of the latest reaction, HRTEM data indicate that the reaction mechanism is more complicated than the simple opening or collapse of interlayers.

3) The HRTEM data explain the XRD characteristics of the studied rocks, documenting the presence of 1 or 2 types of aggregates of mixed-layer crystals and very thin illite crystals. Such thin illite crystals should produce the mixed-layering effect according to the interparticle diffraction concept, and it remains to be discovered why they do not behave as expected.

ACKNOWLEDGMENTS

We thank D. D. Eberl and S. Rimmer for supplying the samples and Eberl and D. Peacor for critical reading and English correction of the manuscript. A. Mizerska handled the manuscript and M. Lemain prepared the photographs. J. Środoń thanks Institut National de la Recherche Agronomique (INRA) for supporting his visits to Versailles, during which the experimental part of this study was completed and the manuscript was discussed.

REFERENCES

Ahn JH, Peacor DR. 1986. Transmission and analytical electron microscopy of the smectite-to-illite transition. Clays Clay Miner 34:165–179.

Allen VT. 1952. Petrographic relations in some typical bauxite and diaspore deposits. Geol Soc Am Bull 63:649–688.

Altaner SP, Hower J, Whitney G, Aronson JL. 1984. Model for K-bentonite formation: Evidence from zoned K-bentonites in the disturbed belt, Montana. Geology 12:412–415.

Amouric M, Olives J. 1991. Illitization of smectite as seen by high-resolution transmission electron microscopy. Eur J Mineral 3:831–835.

Beaufort D, Meunier A. 1983. Petrographic characterization of an argillic hydrothermal alteration containing illite, K-rectorite, K-beidellite, kaolinite and carbonates in a cupromolybdenic porphyry at Sibert (Rhone, France). Bull Mineral 106:535–551.

Bell TE. 1986. Microstructure in mixed-layer illite/smectite and its relationship to the reaction of smectite to illite. Clays Clay Miner 34:146–154.

Bennett P, Siegel DI. 1987. Increased solubility of quartz in water due to complexing by organic compounds. Nature 326:684–686.

Bouchet A, Meunier A, Velde B. 1988. Hydrothermal mineral assemblages containing two discrete illite/smectite minerals. Bull Mineral 111:587–599.

Bustin RM. 1989. Diagenesis of kerogen. In: Hutcheon IE, editor. Burial diagenesis. Montreal: Mineral Assoc Can. p 1–38.

Damberger HH. 1971. Coalification pattern of the Illinois Basin. Econ Geol 66:488–494.

Durand B. 1985. Diagenetic modifications of kerogens. Phil Trans R Soc London A 315:77–88.

Eberl DD, Środoń J. 1988. Ostwald ripening and interparticle diffraction effects for illite crystals. Am Mineral 73: 1335–1345.

Feigenbaum S, Shainberg I. 1975. Dissolution of illite—A possible mechanism of potassium release. Soil Sci Soc Am Proc 39:985–990.

Garrels RM, Mackenzie FT. 1971. Evolution of sedimentary rocks. New York: Norton. 397 p.

Hinsinger P, Elsass F, Jaillard B, Robert M. 1993. Root-induced irreversible transformation of a trioctahedral mica in the rhizosphere of rape. J Soil Sci 44:535–545.

Hower J, Eslinger E, Hower M, Perry E. 1976. Mechanism of burial metamorphism of argillaceous sediment: I. Mineralogical and chemical evidence. Geol Soc Am Bull 87: 725–737.

Huddle JW, Patterson SH. 1961. Origin of Pennsylvanian underclay and related seat rocks. Geol Soc Am Bull 72: 1643–1660.

Hughes RE, Demaris PJ, White WA. 1992. Underclays and related paleosols associated with coals. In: Martini IP, Chesworth W, editors. Weathering, soils and paleosols. Amsterdam: Elsevier. p 501–523.

Inoue A, Utada M, Wakita K. 1992. Smectite-to-illite conversion in natural hydrothermal systems. Appl Clay Sci 7:131–145.

Inoue A, Velde B, Meunier A, Touchard G. 1988. Mechanism of illite formation during smectite-to-illite conversion in a hydrothermal system. Am Mineral 73:1325–1334.

Jahren JS, Aagaard P. 1992. Diagenetic illite–chlorite assemblages in arenites. I. Chemical evolution. Clays Clay Miner 40:540–546.

Jiang W, Peacor D, Merriman RJ, Roberts B. 1990. Transmission and analytical electron microscopic study of mixed-layer illite/smectite formed as an apparent replacement product of diagenetic illite. Clays Clay Miner 38: 449–468.

Klimentidis RE, Mackinnon IDR. 1986. High-resolution imaging of ordered mixed-layer clays. Clays Clay Miner 34: 155–164.

Lanson B. Champion D. 1991. The I/S-to-illite reaction in the late stage diagenesis. Am J Sci 291:473–506.

Nadeau PH, Wilson MJ, McHardy WJ, Tait JM. 1984. Interparticle diffraction: A new concept for interstratified clays. Clay Miner 19:757–769.

Parachoniak W, Środoń J. 1974. The formation of kaolinite, montmorillonite, and mixed-layer montmorillonite-illite during the alteration of Carboniferous tuff (the Upper Silesian Coal Basin). Mineral Polonica 4:37–56.

Paradis S, Velde B, Nicot E. 1983. Chloritoid–pyrophyllite–rectorite facies rocks from Brittany, France. Contrib Mineral Petrol 83:342–347.

Reynolds RC. 1980. Interstratified clay minerals. In: Brindley GW, Brown G, editors. Crystal structure of clay minerals and their X-ray identification. London: Mineral Soc. p 249–303.

Rimmer SM. 1978. Vertical variations in the mineralogical and chemical composition of the underclay of the Herrin (No. 6) coal in southwestern Illinois [M. S. thesis]. Urbana, IL: Univ Illinois. 68 p.

Rimmer SM, Eberl DD. 1982. Origin of an underclay as revealed by vertical variations of mineralogy and chemistry. Clays Clay Miner 30:422–430.

Robert M. 1973. The experimental transformation of mica toward smectite; relative importance of total charge and tetrahedral substitution. Clays Clay Miner 21:167–174.

Robert M. 1987. Some general aspects of K dynamics and new trends in soil mineralogy. Trans 13 Congr Int Soc Soil Sci; 1986; Hamburg. p 1122–1132.

Romero R, Robert M, Elsass F, Garcia C. 1992. Evidence by electron microscopy of weathering microsystems in soil formations developed from crystalline rocks. Clay Miner 27:21–33.

Scott AD. 1987. Mechanisms of potassium release by soil minerals. Trans 13 Congr Int Soc Soil Sci; 1986; Hamburg. p 1144–1154.

Small JS. 1995. Experimental and modeling studies of the pH control of the smectite-to-illite reaction, Programs and Abstracts. 5th Goldschmidt Conf; 1995; State College, PA. p 88.

Środoń J. 1972. Mineralogy of coal–tonstein and K-bentonite from coal-seam no. 610, Bytom Trough (Upper Silesian Coal Basin, Poland). Bull Acad Polon Sci, Ser Sci Terre 20:155–164.

Środoń J. 1976. Mixed-layer smectite/illites in the bentonites and tonsteins of the Upper Silesian Coal Basin. Prace Mineral 49:1–84.

Środoń J. 1979. Correlation between coal and clay diagenesis in the Carboniferous of the Upper Silesian Coal Basin. Proc 6th Int Clay Conf; 1978; Oxford. Amsterdam: Elsevier. p 251–260.

Środoń J. 1981. X-ray identification of randomly interstratified illite/smectite in mixtures with discrete illite. Clay Miner 16:297–304.

Środoń J. 1984. X-ray powder diffraction identification of illitic materials. Clays Clay Miner 32:337–349.

Środoń J, Andreoli C, Elsass F, Robert M. 1990. Direct HRTEM measurement of expandability of mixed-layer illite/smectite in bentonite rock. Clays Clay Miner 38:373–379.

Środoń J, Eberl DD. 1984. Illite. In: Bailey SW, editor. Micas. Rev Mineral 13. Washington, DC: Mineral Soc Am. p 495–544.

Środoń J, Elsass F, McHardy WJ, Morgan DJ. 1992. Chemistry of illite/smectite inferred from TEM measurements of fundamental particles. Clay Miner 27:137–158.

Środoń J, Elsass F. 1994. Effect of the shape of fundamental particles on XRD characteristics of illitic minerals. Eur J Mineral 6:113–122.

Suarez M, Robert M, Elsass F, Pozas JM. 1994. Evidence of a precursor in the neoformation of palygorskite—New data by analytical electron microscopy. Clay Miner 29:255–264.

Sucha V, Środoń J, Elsass F, McHardy WJ. 1996. Particle shape versus coherent scattering domain of illite/smectite: Evidence from HRTEM of Dolna' Ves clays. Clays Clay Miner 44:665–671.

Taguchi K, Shimoda S, Itihara Y, Imoto N, Ishiwatari R, Shimoyama A. 1986. Relationship of organic and inorganic diagenesis of neogene Tertiary rocks, Northeastern Japan. In: Gautier DL, editor. Roles of organic matter in sediment diagenesis. Soc Econ Paleontol Mineral Spec Publ 38. p 47–64.

Tomita K, Dozono M. 1972. Formation of an interstratified mineral by extraction of potassium from mica with sodium tetraphenylboron. Clays Clay Miner 20:225–231.

Tributh H, Boguslawski E, Lieres A, Steffens D, Mengel K. 1987. Effect of potassium removal by crops on transformation of illitic clay minerals. Soil Sci 143:404–409.

Vali H, Koster HM. 1986. Expanding behaviour, structural disorder, regular and random irregular interstratification of 2:1 layer-silicates studied by high-resolution images of transmission electron microscopy. Clay Miner 21:827–859.

White JL. 1951. Transformation of illite into montmorillonite. Soil Sci Soc Am Proc 15:129–133.

(*Received 16 May 1995; accepted 11 July 1996; Ms. 2648*)